Michigan State University

National Superconducting Cyclotron Laboratory

RESIDUE TEMPERATURES AND THE NUCLEAR EQUATION OF STATE

H.M. XU, P. DANIELEWICZ, and W.G. LYNCH

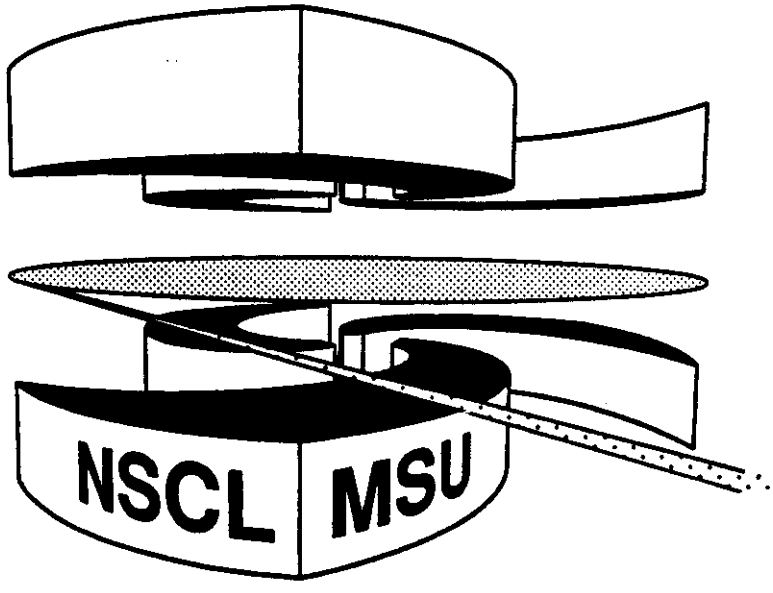

MSUCL-816 **JANUARY 1992**

MSUCL-816
January, 1992

Residue Temperatures and the Nuclear Equation of State

H.M. Xu[1,2], P. Danielewicz[1], and W.G. Lynch'

[1] National Superconducting Cyclotron Laboratory and
Department of Physics, Michigan State University
East Lansing, Michigan 48824
[2] Cyclotron Institute, Texas A&M University, College Station, Texas, 77843

Abstract

Excitation energies are calculated for heavy residues produced in central $^{40}Ar + ^{124}Sn$ collisions for a range of incident energies and impact parameters using the BUU transport equation. These excitation energies are evaluated at freezeout times determined from the time dependence of the thermal excitation energy and the nucleon emission rate. Both the thermal excitation energies and temperatures,' obtained assuming Fermi gas level densities, are sensitive to the nuclear equation of state and the impact parameter. Surprisingly little sensitivity is observed to the in-medium nucleon-nucleon cross section.

Intermediate energy nucleus-nucleus collisions provide excellent opportunities for producing hot nuclear systems [1-25] at excitation energies and temperatures near the values beyond which metastable nuclei cannot exist.[16-21] Many experimental investigations suggest a limiting temperature in the range of T=4-6 MeV.[4-11] Such observations could reflect either the thermal instabilities of metastable hot nuclei[16-21] or some dynamical limits to the energy which can be deposited into these residues via the reactions being studied.[23-24]

To investigate the possible dynamical limits to the excitation energies of hot residual nuclei, and the sensitivity of residue excitation energies to the nuclear equation of state and the in-medium nucleon-nucleon cross section, calculations were performed with an improved Boltzmann-Uehling-Uhlenbeck (BUU) model for ^{40}Ar+^{124}Sn reactions at a variety of incident energies. In these calculations, the BUU equation [26,27]

$$\frac{\partial f_1}{\partial t} + \mathbf{v}\cdot\nabla_r f_1 - \nabla_r U\cdot\nabla_p f_1 = \frac{4}{(2\pi)^3}\int d^3k_2 d\Omega \frac{d\sigma_{nn}}{d\Omega} v_{12} \times[f_3 f_4(1-f_1)(1-f_2) - f_1 f_2(1-f_3)(1-f_4)] \quad (1)$$

was solved via the Lattice Hamiltonian method of Lenk and Pandharipande [28,29]. In Eq. (1), f is the Wigner transform of the one body density matrix, $\frac{d\sigma_{nn}}{d\Omega}$ and v_{12} are the in-medium nucleon-nucleon cross section and relative velocity for the colliding nucleons, and U is the total mean-field potential. For the present calculations, U consisted of the Coulomb potential and a nuclear potential which contained both isoscalar and symmetry terms. Calculations were performed for two different isoscalar mean fields, one with a stiff EOS with a compressibility of K=380 MeV and the other with a soft EOS with a compressibility of K=200 MeV. For simplicity, $\frac{d\sigma_{nn}}{d\Omega}$ was chosen to be isotropic and energy independent. Both the mean field and the Pauli- blocking factors in the collision integral were averaged over ensembles consisting of 80 parallel simulations.

Calculations were performed on a grid with lattice spacings of 1 fm for elapsed times of 200 fm/c after initial contact between the projectile and target nuclei. To determine the thermal excitation energy of the residue at the end of the pre-equilibrium cascade, the total energy, E_{tot}, was decomposed into collective, E_{coll}, and internal, E_{int}, components, [23]

$$E_{tot} = E_{coll} + E_{int}. \tag{2}$$

The total energy E_{tot} is obtained by summing the kinetic and potential energies of the test particles.[28] The collective energy is estimated by

$$E_{coll} = \frac{1}{2} m \int \frac{\vec{j}^2(\vec{r})}{\rho(\vec{r})} d^3r, \tag{3}$$

where

$$\rho(\vec{r}) = \frac{4}{(2\pi\hbar)^3} \int f(\vec{r}, \vec{p}, t) d^3p, \tag{4}$$

is the nucleon density,

$$\vec{j}(\vec{r}) = \frac{4}{(2\pi\hbar)^3} \int \frac{\vec{p}}{m} f(\vec{r}, \vec{p}, t) d^3p, \tag{5}$$

is the local collective current field, and m is the nucleon mass. The internal energy E_{int} was decomposed into a thermal excitation energy E^*_{the} and an internal energy $E_{int}(T = 0, A_{res})$:

$$E_{int} = E^*_{the} + E_{int}(T = 0, A_{res}), \tag{6}$$

Here $E_{int}(T = 0, A_{res})$ includes the potential energy and the kinetic energy of Fermi motion for a cold nuclear system of A_{res} nucleons at the same density.[23,29]

The time evolution of the various contributions to the total energy are shown in Fig. 1 for ^{40}Ar+^{124}Sn collisions at E/A = 65 MeV and b=0 with the stiff (upper panel) and soft (lower panel) equations of state. In the calculation with the stiff EOS, the nuclear potential

energy (bottom curve in each panel) has a minimum at t $\approx$ 30 fm/c, where projectile and target nucleons are strongly overlapping, followed by rapid increase to a maximum at t $\approx$ 70 fm/c as the system expands to lower density. The potential subsequently decreases to a minimum at about t = 120 fm/c as the residue relaxes to a spherical configuration. In contrast, the later expansion and contraction stages of the reaction proceed much more slowly and the potential energy reaches a minimum at about t = 160 fm/c, for calculations with the soft EOS. This difference reflects the fact that forces which restore density modulations are weaker for the soft EOS and, therefore, adjustments of the density distributions, governed by the speed of sound, are slower. The differences between successive lines in each panel of the figure provide successively: 1) the Coulomb potential energy, 2) the Fermi energy of a zero temperature nuclear system at the same density, 3) the energy of free nucleons, 4) the collective energy, E_{coll} , of nucleons residing in regions of density $\rho(\vec{r}) \geq 0.1\rho_o$, and 5) the thermal energy, E^*_{the}. Two maxima are observed in the thermal energy. The global maximum at t $\approx$ 30 fm/c is an artifact of the initial momentum distributions, in which the longitudinal velocities of the projectile and target nuclei cancel each other, causing a minimum in the computation of the collective energy. The second maximum at t $\approx$ 120 fm/c for the stiff EOS, and t $\approx$ 160 fm/c for the soft EOS, occurs after the initial pre-equilibrium stages of the collision; this maximum provides one estimate of the maximum or initial thermal excitation energy of the reaction residue. The corresponding time provides an estimate of the freezeout time t_{fre} which marks the cessation of pre-equilibrium emission. After this second maximum the thermal excitation energy decreases slowly with time reflecting the well studied evaporative cooling mechanisms operant in hot equilibrated nuclei.

More direct information about the freezeout time is provided by the nucleon emission rates, shown in the upper panels of Fig. 2 for the calculations shown in Fig. 1. Freezeout

times determined from the second maximum in the thermal energy are indicated by the vertical dash-dotted lines. For both the stiff (left panels) and the soft (right panels) equations of state, one observes large emissions rates at t $\approx$ 50 - 80 fm/c. These large emission rates reflect the fast pre-equilibrium emission that occurs when these systems are at their minimum densities. The nucleon emission rates attain local minima at the freezeout times determined from the maxima in the thermal energies, providing additional support for those determinations of the freezeout times. After t_{fre}, the emission rates increase somewhat, but remain small reflecting the slower emission rates typical of evaporative processes.

The bottom panels of Fig. 2 show the quadrupole moment of the momentum distribution Q_{ZZ} [30-32]

$$Q_{ZZ}(t) = \frac{1}{(2\pi\hbar)^3} \int d^3r d^3p (2p_z^2 - p_x^2 - p_y^2) f(\vec{r}, \vec{p}, t) \tag{7}$$

which has been proposed as a measure of the degree of equilibration of the colliding system. Clearly, at the freezeout times determined from the thermal energy, Q_{ZZ} is significantly reduced from its initial value and is close to zero, as expected for an equilibrated system. Determinations of precise freezeout times from Q_{ZZ} are difficult, however, since Q_{ZZ} continues to oscillate about zero for a long time, reflecting the existence of macroscopic quadrupole vibrations.

Fig. 3 shows the predicted thermal excitation energy/nucleon as a function of the impact parameter for ^{40}Ar+^{124}Sn collisions at E/A=35 MeV (top window) and E/A=65 MeV (bottom window), respectively. A comparison of the thermal excitation energies calculated for the two equations of state and $\sigma_{NN} = \int \frac{d\sigma_{nn}}{d\Omega} d\Omega$ =41 mb are shown in the left hand panels. The thermal excitation energies calculated for the stiff EOS (open circles) are significantly larger than those calculated for the soft EOS (solid circles). This dependence

can be attributed to the later freezeout time for calculations with the soft EOS, since it allows a longer time during which energy can be carried away by pre- equilibrium nucleon emission. The thermal excitation energies also depend more strongly upon impact parameter at the higher incident energy, where the target nucleus is less effective in capturing nucleons from the projectile, than at E/A=35 MeV. The right hand side of the figure shows the sensitivity of the residue thermal excitation energies to the in-medium nucleon-nucleon cross section for calculations assuming a soft equation of state. Calculations with σ_{NN} = 20 mb (open circles) are slightly larger than the corresponding calculations with $\sigma_{NN} = 41$ mb (solid circles). This difference stems mainly from a higher nucleon emission rate and therefore cooling rate for the calculations with the larger nucleon-nucleon cross section. For the calculations at E/A=65 MeV, this difference is comparable, however, to the uncertainty in the calculated thermal excitation energy $\delta E^*/A = 0.3$ MeV due to uncertainties in defining the freezeout time.

The top panel of Fig. 4 shows the energy dependence of the thermal excitation energy/nucleon at b=0 fm for the two equations of state and $\sigma_{NN} = 41$ mb. The bottom panel shows corresponding estimates of the residue temperatures, calculated by integrating the Fermi-gas expression $\varepsilon^*(T, \varepsilon_F(\rho))$ over the density distributions and equating the integrated value to the thermal energy from the numerical simulations. ($\varepsilon_F(\rho)$ is the Fermi energy for a nuclear system at density ρ.) Assuming equal Fermi energies for protons and neutrons and the low temperature limit, this procedure yields:

$$E^*_{the} = aT^2 = \{\frac{m}{3\hbar^2}(\frac{3\pi^2}{2})^{1/3} \int d^3r \rho^{1/3}(\vec{r})\} T^2 \qquad (8)$$

where the integration is performed over the volume of the reaction residue, defined by the requirement $\rho(\vec{r}) \geq 0.1\rho_o$. (Except at the highest incident energies, E/A $\geq$ 65 MeV, eq. (8) provides a level density parameter close to A/10.) In both panels of the figure,

the dashed lines represent calculations using the stiff EOS and the solid lines represent calculations using the soft EOS. Both equations of state predict a gradual increase in the residue thermal excitation energies and temperatures as the incident energy is raised from E/A = 30 MeV to 85 MeV. The rate of increase, however, becomes very small at the highest incident energies and the calculated temperatures are nearly constant at E/A $\geq$ 65 MeV.

A saturation has been reported in the excitation energies deduced from measurements of the multiplicities of neutrons and α particles.[2,3] Since pre-equilibrium emission carries away more nucleons in our calculations than assumed in the analysis of neutron and α particle multiplicities, we do not know whether our calculations are truly comparable to the data, and therefore, we refrain from making this comparison. Limiting temperatures have also been deduced from the energy spectra of light particles [4-10] and from the relative populations of excited states of emitted complex fragments.[11-15] In the bottom panel, we include the temperatures extracted from energy spectra of light charged particles by refs. [7] (open diamond), [9] (open cross), [4] (solid triangles), [6] (open square), [10] (open triangle); neutron energy spectra by ref. [5] (star), and the emission temperatures extracted from excited states by refs. [11] (solid- circles and crosses), [12] (open circle), [13] (solid diamond), and ref. [14] (solid square), because such temperatures have proven relatively insensitive to the total mass of the colliding system. Except for the few data points represented by an open diamond and an open cross, the calculated temperatures are similar to the measured values. This comparison must, nevertheless, be regarded as speculative, because measured temperatures are expected to be strongly impact parameter dependent and the influence of impact parameter averaging on these measurements is poorly understood.

In summary, thermal excitation energies of residues have been calculated as functions

of the impact parameter for central $^{40}Ar+^{124}Sn$ collisions over a range of incident energies. These thermal excitation energies are evaluated at freezeout times determined from the time dependences of the thermal excitation energy and the emission rate of nucleons. Both these thermal excitation energies and temperatures, obtained assuming Fermi gas level densities, are sensitive to the nuclear equation of state and the impact parameter. Surprisingly little sensitivity is observed to the in-medium nucleon-nucleon cross section.

We would like to acknowledge many fruitful discussions with G.F. Bertsch, C.K. Gelbke, M. Tohyama, and M.B. Tsang. W.G. Lynch acknowledges receipt of an NSF Presidential Young Investigator Award. This work was supported by the National Science Foundation under Grant numbers PHY-86-11210, and PHY- 89-05933, and by the Department of Energy under Grant No. DE-FG05-86ER40256.

References

[1] C.K. Gelbke and D.H. Boal, Prog. Part. Nucl. Phys. **19** (1987) 33.

[2] J. Galin, Nucl. Phys. **A488**(1988) 297c.

[3] D.X. Jiang, *et al*, Nucl. Phys. **A503** (1989) 560.

[4] S. Song, *et al*, **130B** (1983) 14.

[5] D. Hilscher, *et al*, Phys. Rev. **C36** (1987) 208.

[6] D. Jacquet, *et al*, Phys. Rev. **C32** (1985) 1594; D. Jacquet, Thesis, Orsay, 1987.

[7] R. Wada, *et al*, Phys. Rev. **C39** (1988)497.

[8] M. Gonin, *et al*, Phys. Lett. **B217** (1988) 406.

[9] K. Hagel, *et al*, Nucl. Phys. **A486** (1988) 429.

[10] A. Chbihi, *et al*, Phys. Rev. **C43** (1991) 666.

[11] Z. Chen, *et al*, Phys. Rev. **C36** (1987) 2297; Nucl. Phys. **A473** (1987) 564.

[12] H.M. Xu, *et al*, Phys. Rev. **C40** (1989) 186; Phys. Lett. **B182** (1986) 155.

[13] C. Bloch, *et al*, Phys. Rev. **C36** (1987) 203.

[14] T.K. Nayak, *et al*, to be published.

[15] G. Kunde, *et al*, to be published.

[16] H. Sagawa, and G.F. Bertsch, Phys. Lett. **155B** (1985) 11.

[17] S. Levit and P. Bonche, Nucl. Phys. **A437**(1984) 426; J. Besprosvany and S. Levit, Phys. Lett. **B217** (1989) 1.

[18] D.H.E. Gross, *et al*, Phys. Lett. **B203** (1988) 26.

[19] J. Bondorf *et al*, Phys. Lett. **162B** (1985) 30; Nucl. Phys. **A443** (1985) 321.

[20] D.H. Boal, *et al*, Phys. Rev. Lett. **62** (1989) 737.

[21] W.A. Friedman, Phys. Rev. Lett. **60** (1988) 2125.

[22] S. Shlomo and J.B. Natowitz, Phys. Lett. **252B** (1990) 187.

[23] B. Remaud, *et al*, Nucl. Phys. **A488** (1988) 423c.

[24] E. Suraud, *et al*, Phys. Lett. **B229** (1989) 359.

[25] S. Bhattacharya, *et al*, Phys. Rev. Lett. **62** (1989) 2589.

[26] G.F. Bertsch and S. Das Gupta, Phys. Rep. **160** (1988) 189, and references therein.

[27] J. Aichelin and G. Bertsch, Phys. Rev. **C331** (1985) 1730.

[28] R.J. Lenk and V.R. Pandharipande, Phys. Rev. **C39**, 2242(1989).

[29] H.M. Xu,*et al*, Phys. Rev. Lett. **65** (1990) 843; Phys. Lett. **B261** (1991) 240.

[30] W. Cassing, Z. Phys. **A327** (1987) 447.

[31] K. Niita, *et al*, Nucl. Phys. **504** (1989) 391.

[32] W. Bauer, Phys. Rev. Lett. **61** (1988) 2534.

Figure Captions

Fig. 1: Decomposition of the excitation energy per nucleon as a function of time for central ^{40}Ar+^{124}Sn collisions at E/A=65 MeV, for the stiff (top window) and the soft EOS (bottom). The differences between subsequent lines are respectively: Coulomb energy, Fermi energy, kinetic energy of emitted particles, collective energy of bound nucleons, and thermal energy. The freezeout time is indicated with a dash-dotted line.

Fig. 2: The emission rate of nucleons (top panels), the quadrupole moment, Q_{ZZ}, (bottom panels), as a function of time for both the stiff EOS (left panels) and the soft EOS (right panels). The vertical dash-dotted lines indicate the freezeout times discussed in the text. The dashed lines in the bottom panels include calculations for all nucleons, while the solid lines include only nucleons bound in residues.

Fig. 3: Sensitivities of the temperature to the EOS (left panels) and σ_{NN} (right panels) for ^{40}Ar+^{124}Sn collisions at E/A=35 MeV (top panels) and 65 MeV (bottom panels). Details are discussed in the text.

Fig. 4: Dependence of thermal excitation energies (top panel) and temperatures (bottom) on the incident energy for ^{40}Ar+^{124}Sn collisions at b=0. The dashed lines are results for the stiff EOS and the solid lines are results for the soft EOS. The other symbols in the bottom panel are experimental data discussed in the text.

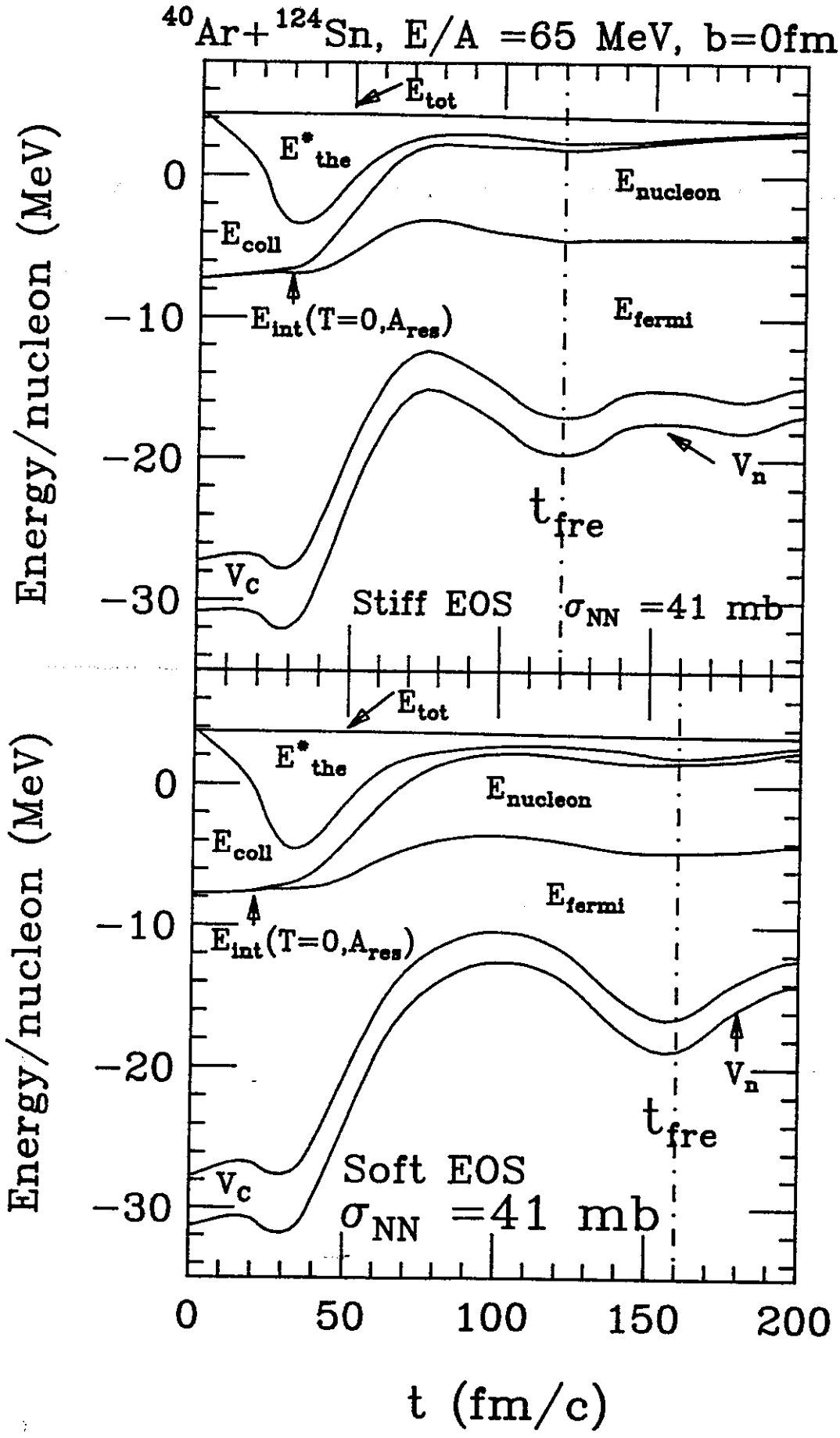
^{40}Ar+^{124}Sn, E/A =65 MeV, b=0fm
E_{tot}
E^*_{the}
$E_{nucleon}$
E_{coll}
$E_{int}(T=0,A_{res})$
E_{fermi}
V_n
t_{fre}
V_c
Stiff EOS
σ_{NN} =41 mb
Soft EOS
σ_{NN} =41 mb
Energy/nucleon (MeV)
t (fm/c)
0
50
100
150
200
−10
−20
−30

Fig. 1

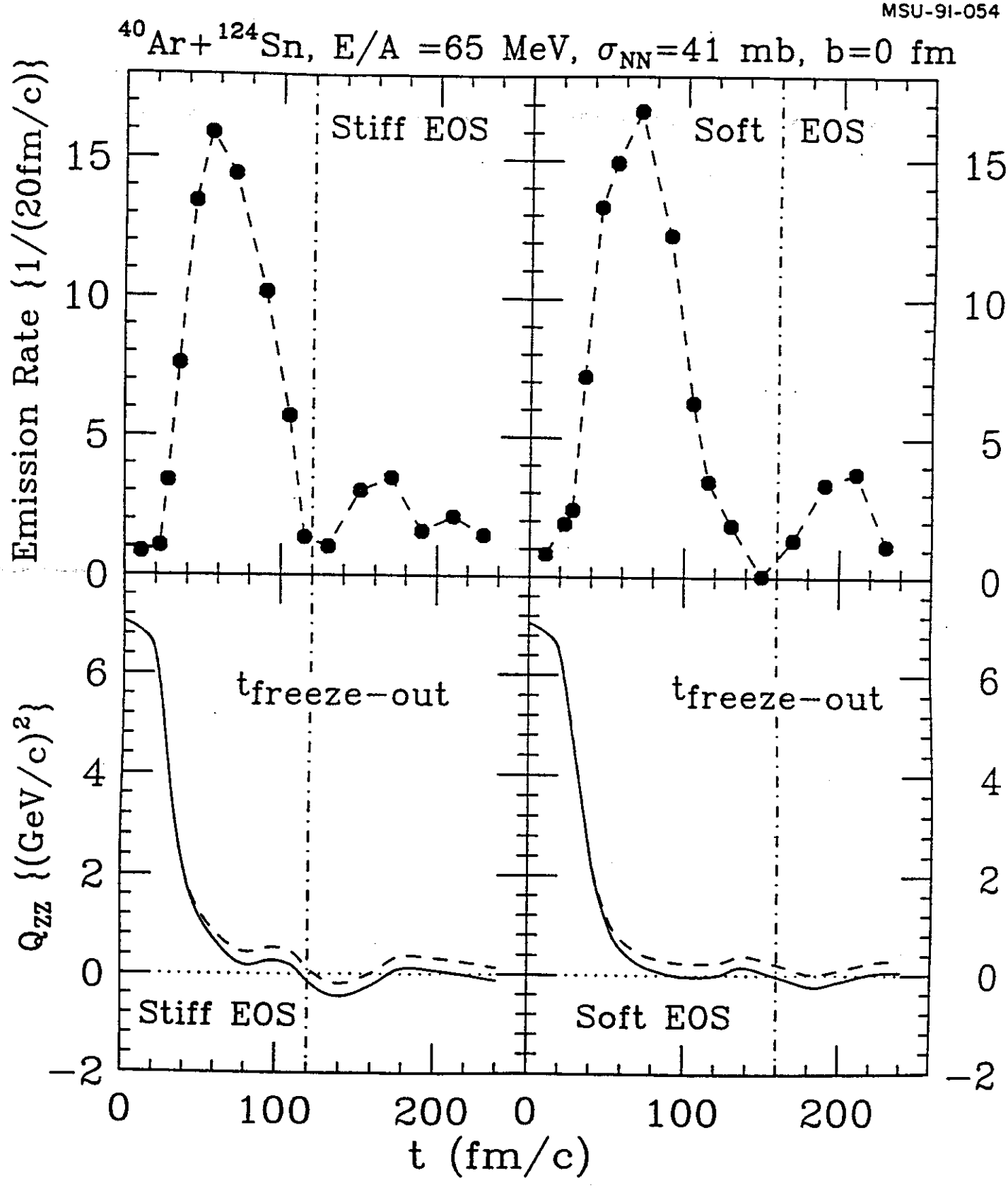
^{40}Ar+^{124}Sn, E/A =65 MeV, σ_{NN}=41 mb, b=0 fm
Stiff EOS
Soft EOS
Emission Rate {1/(20fm/c)}
$t_{freeze-out}$
$t_{freeze-out}$
Q_{zz} {(GeV/c)^2}
Stiff EOS
Soft EOS
t (fm/c)

Fig. 2

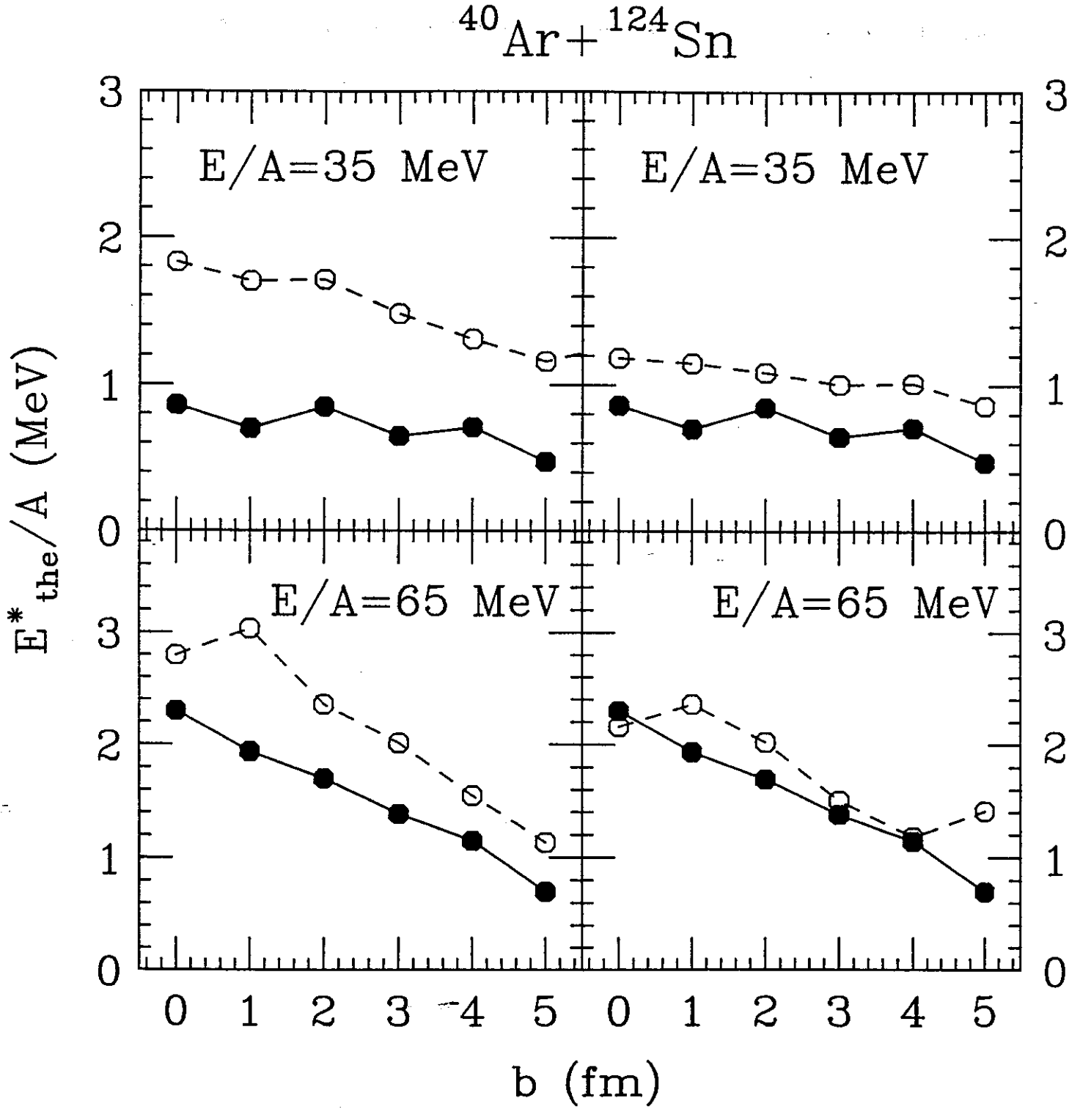
$^{40}Ar+^{124}Sn$
E/A=35 MeV
E/A=35 MeV
E/A=65 MeV
E/A=65 MeV
E^*_{the}/A (MeV)
b (fm)
0
1
2
3
4
5

Fig. 3

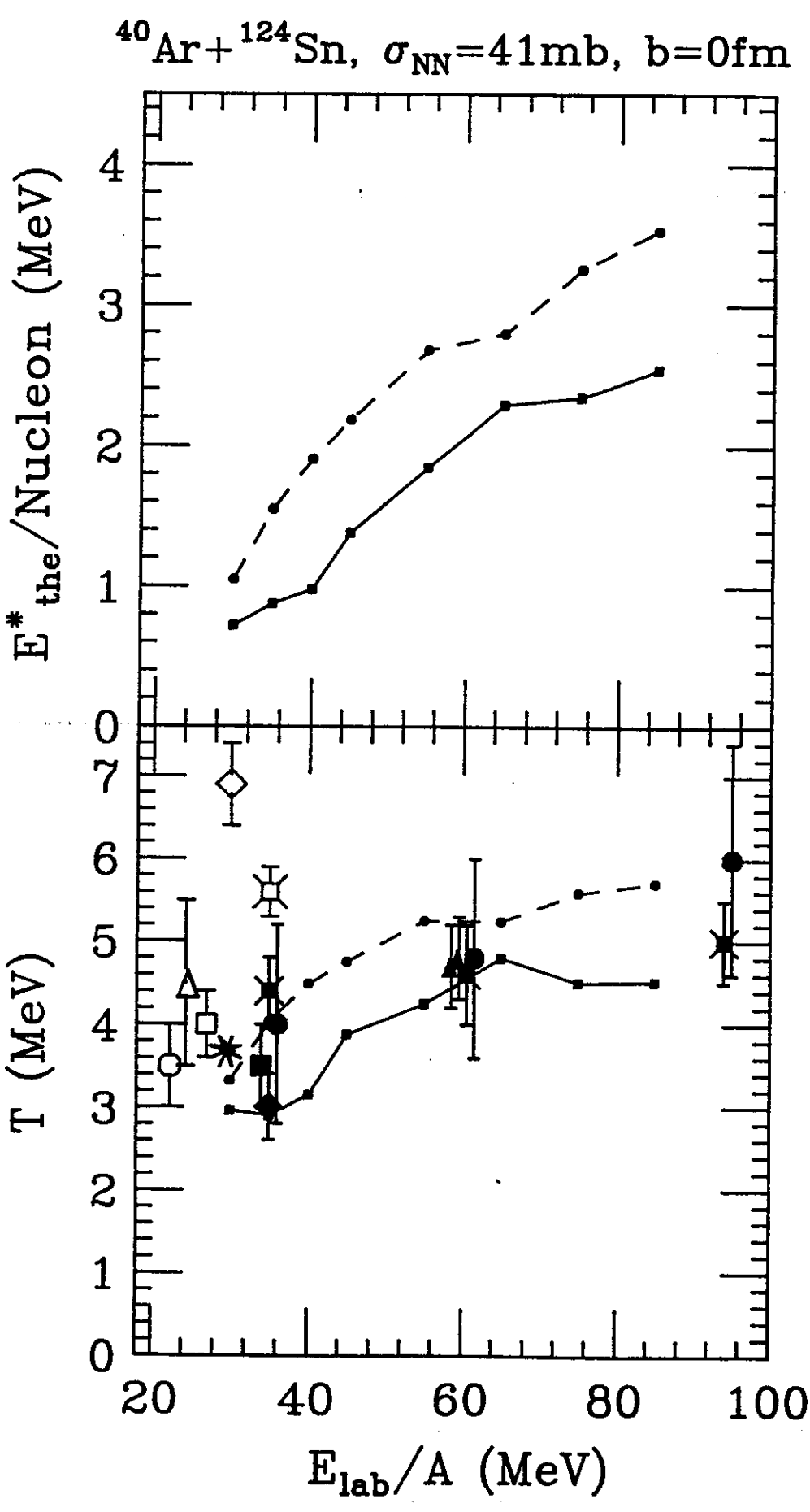
^{40}Ar+^{124}Sn, σ_{NN}=41mb, b=0fm
E^*_{the}/Nucleon (MeV)
T (MeV)
E_{lab}/A (MeV)
0
1
2
3
4
5
6
7
20
40
60
80
100

Fig. 4